Available online at www.sciencedirect.com

ScienceDirect

journal homepage: www.elsevier.com/locate/he

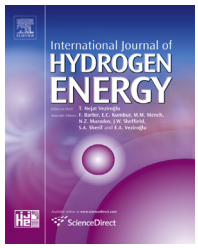

Solar steam reforming for enriched methane production: Reactor configurations modeling and comparison

M. De Falco [a,*], G. Caputo [b], S. Frattari [c], F. Gironi [c], M.C. Annesini [c]

[a] Facoltà di Ingegneria, Università Campus Bio-Medico di Roma, Via Alvaro del Portillo 21, 00128, Roma, Italy
[b] ENEA Research Center "Casaccia", via Anguillarese 301, 00123, Roma, Italy
[c] Dipartimento di Ingegneria Chimica Materiali e Ambiente, Università "La Sapienza" di Roma, via Eudossiana 18, 00184, Roma, Italy

ARTICLE INFO

Article history:
Received 4 April 2014
Received in revised form
10 June 2014
Accepted 27 June 2014
Available online 29 July 2014

Keywords:
Solar steam reforming
Enriched methane
Concentrating solar power plant
Hydrogen production
Reactor modeling

ABSTRACT

A solar low-temperature steam reforming process for the production of an Enriched Methane (EM) mixture composed by CH_4 and H_2 (20%vol) exploiting the solar energy stored in a Molten Salt stream heated up by a Concentrating Solar Plant (MS-CSP) is presented and simulated through a two-dimensional steam reforming reactor model.

Two configurations are considered and compared: the Integrated Heat Exchanging (IHE) configuration, where the steam reformers are tubes-and-shell reactors continuously heated up by the hot MS stream, and the External Heat Exchanging (EHE) configuration composed by a series of heat exchangers and insulated reformers where the reactions are adiabatically driven.

The effect of the main operating conditions as Gas Hourly Space Velocity (GHSV), inlet reactor temperature and reactant mixture composition is assessed for both the configurations, demonstrating the process feasibility. Furthermore, in order to increase the process performance, an electrical power generation unit is also included, exploiting the sensible heat of the residual MS stream after the EM production unit: in this case, with a feed of 2000 Nm^3/h of natural gas, about 6130 Nm^3/h of enriched methane and 475 kW_{el} are produced with the EHE configuration, while 3720 Nm^3/h and 585 kW_{el} are obtained with IHE configuration.

Introduction

Enriched methane (EM) is a gas mixture composed by hydrogen (10–30% vol) and methane, able to be used as feedstock in the traditional natural gas internal combustion engines (NG-ICE) without the need of expensive technical modifications and leading to an improvement of the engine efficiency and to a reduction of CO, CO_2 and un-burned emissions [1–6]. Therefore, the EM is a hybrid fuel composed by an amount of fossil fuel (natural gas) and a share of hydrogen, produced by exploiting renewable energy as solar

* *Corresponding author*. Tel.: +39 347 6809041.
E-mail addresses: m.defalco@unicampus.it, marcello.defalco@gmail.com (M. De Falco).
http://dx.doi.org/10.1016/j.ijhydene.2014.06.151

energy, wind, hydroelectric energy or biomass: its combustion leads to the emission of pollutants and Green House Gases (GHGs) for the fossil fuel share, while hydrogen combustion produces only water. Consequently, the greater the amount of hydrogen in EM composition, the greater the emission reduction, as shown in Fig. 1 where the mass reduction of CO_2 emission is depicted in function of H_2 volumetric composition.

Moreover, EM can be stored in the standard compressed natural gas storage systems and, if the H_2 content is limited at 17%, the mixture can be distributed by means of the medium pressure NG grid, immediately after the pressure reduction stations [7].

Basically, EM solves the main technological problems (production, storage, distribution and use) which are hindering the hydrogen diffusion as energy vector: EM can be considered as a first technological steps towards the "hydrogen economy" development [8] since it can be applied in the next years using all the infrastructure already available for the natural gas, with immediate environmental and energetic benefits.

Many processes are proposed in the literature to produce EM exploiting renewable energies [9–13]. Here, a solar-driven steam reforming process [12] is modeled and assessed. Since the steam reforming is the most important massive H_2 production route [14] and a wide industrial experience on the technology is already available, the solar reforming seems to be the most competitive process to produce large amount of EM mixture.

Steam reforming is based on the following reactions:

$$CH_4 + H_2O \leftrightarrow CO + 3H_2 \quad \Delta H^0_{298K} = 206 \frac{kJ}{mol} \tag{1}$$

$$CO + H_2O \leftrightarrow CO_2 + H_2 \quad \Delta H^0_{298K} = -41 \frac{kJ}{mol} \tag{2}$$

The first one is the Steam Reforming reaction (SR), strongly endothermic and very fast over Ni-based catalyst, so that equilibrium conditions are quickly approached; the second one is the exothermic Water Gas Shift (WGS) reaction, that produces a further amount of hydrogen converting CO into CO_2.

In the industrial reforming plants for hydrogen production, the reactors operate at high temperature (850–1000 °C) in order to achieve high hydrogen yield (methane conversion > 90%); to reach these temperatures, reactors are heated inside furnaces. Then, H_2 is separated from the outlet stream by using standard separation processes (Pressure Swing Adsorption, ammine absorption, etc).

If an EM stream has to be produced instead of pure hydrogen, the traditional process unit is modified as follow:

1. the operating temperature is reduced (~500 °C) since a low methane conversion is required (<35%);
2. the H_2 produced through the reforming process has not to be separated from CH_4, avoiding the installation of expensive separation units. On the contrary, a separation unit to remove carbon dioxide may be required.

From these considerations, it has been proposed to produce EM by coupling a low-temperature steam reforming with a MS-CSP (Molten Salt based Concentrating Solar Power) plant [12,13], by which a molten salt stream is heated up to 550 °C (a temperature suitable for the low temperature steam reforming) thanks to parabolic mirrors able to concentrate solar rays on a receiver tube.

The hot molten salt stream is stored in hot storage systems, properly designed in order to maximize the "capacity factor" (i.e. productivity) of the solar plant and to dump the effects of the instantaneous solar radiation availability and fluctuations [15–17]. Then, the hot stream provides all the process heat duties (endothermic reactions thermal duty, steam generation, feedstock pre-heating). Fig. 2 shows a plant conceptual layout.

The core of the chemical process is the low-temperature steam reforming reactor (LTSRR), which has to be properly modeled. In the present paper two different reactor configurations are proposed and compared:

- Internal Heat Exchanging (IHE) configuration, where the reactants, preheated in an external heat exchanger, are fed to a tubes-and-shell reactor heated up by the hot molten salt stream, fed to the shell;
- External Heat Exchanging (EHE) configuration, composed by a series of heat exchanger + reformer modules. The feedstock is firstly heated in an external heat exchanger by

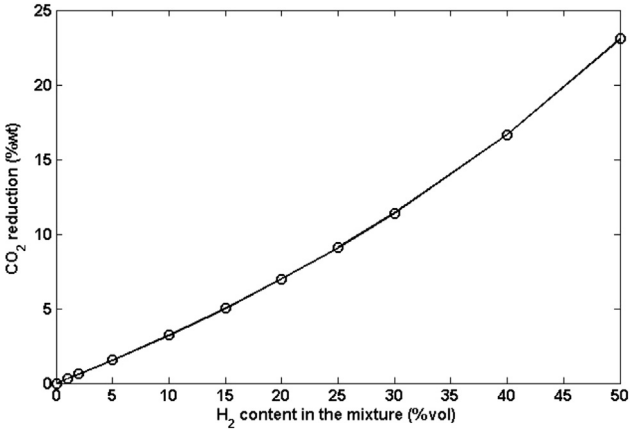

Fig. 1 – CO_2 reduction (%wt) vs. EM H_2 volumetric content during EM combustion in NG-ICE.

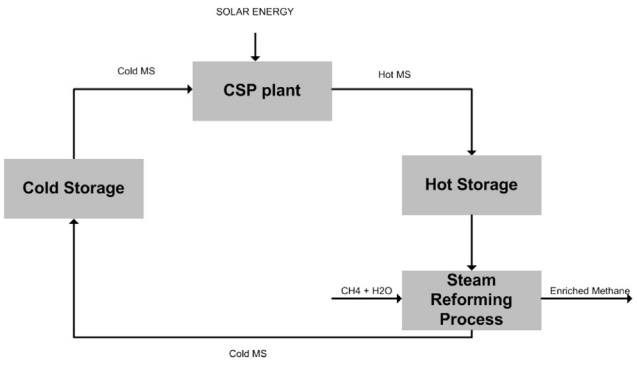

Fig. 2 – Steam reforming coupled with MS-CSP plant conceptual layout.

the hot molten salt stream and then it is partially converted in a first adiabatic reformer. The outlet stream is heated up again and fed to the second reactor. The final natural gas conversion, and consequently the EM composition, depends on the number of assembled exchanger + reactor modules.

In the following, the IHE and EHE configurations are described in detail; then the IHE and EHE solar reactors are modeled and simulated, allowing to compare the process results.

Process configurations

Internal Heat Exchanging configuration

In the IHE configuration, the reactor is tubes-and-shell shaped and the reactant mixture is fed into the tubes, while the hot molten salt stream is sent to the shell. Obviously, molten salt could be sent in co- or in counter-current: in the following, only the co-current configuration is considered since it leads to a better thermal behavior [12].

Fig. 3 shows a simplified process scheme of the IHE configuration.

Basically, the process is composed by:

- a pre-heating heat exchanger (E-1), where the reactant mixture is heated up to the inlet reaction temperature $T_{R,in}$;
- the tubes-and-shell reactor (R-1), where the reforming reactions are supported by the heat provided by the molten salt;
- a low temperature WGS reactor (R-2), where the content of CO in the products mixture is further reduced by supporting at 200 °C the WGS reaction (2);
- a H_2O condensation unit (E-2 and S-1) to separate the unreacted water;
- a PReferential Oxidation (PROX) unit (R-3) for the final abatement of the residual CO traces;
- an absorption process using ammine (MDEA) solution R-4) to separate CO_2;
- a mixer, just before the battery limits, where a CH_4 stream is added to modulate the EM composition.

It is assumed that the heat duty to produce the reactant steam is recovered from the H_2O condensation in E-2 and from the exothermic WGS reaction in R-2, while the hot molten salt stream supplies both the pre-heating and reforming reaction duties.

At the end, the gas mixture, composed by CH_4 and H_2, is sent to the NG grid or to the storage.

The molten salt stream, after supplying the process heat duty, is sent to an electricity generation unit, to recover the residual sensible heat. Then, the cold salt (290 °C) is collected in a cold storage tank and sent again to the CSP.

External Heat Exchanging configuration

In the EHE configuration, shown in Fig. 4, the reactor is composed by a series of heat exchangers (E-1, E-2, …, E-n), where the hot molten salt heats the reactant mixture up to inlet reaction temperature $T_{R,in}$, and adiabatic reactors (R-1, R-2, …, R-n) where the reactions (1–2) are supported.

The stream from the last reactor follows the same process of the IHE configuration, i.e. it is sent the WGS unit to reduce

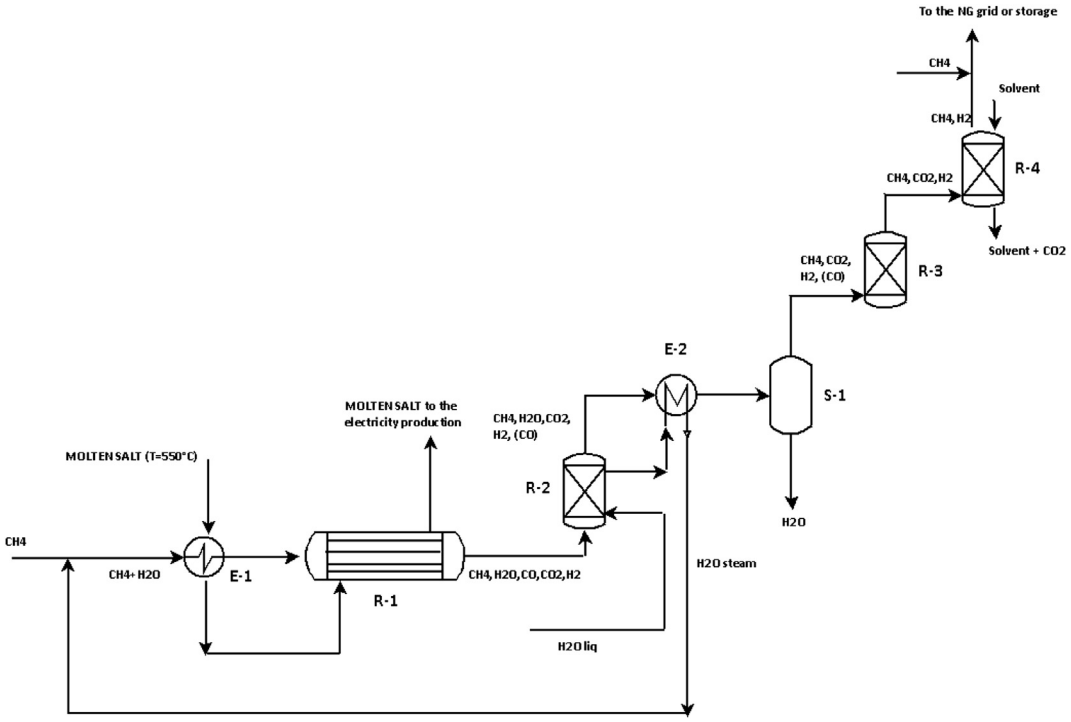

Fig. 3 – IHE configuration process scheme.

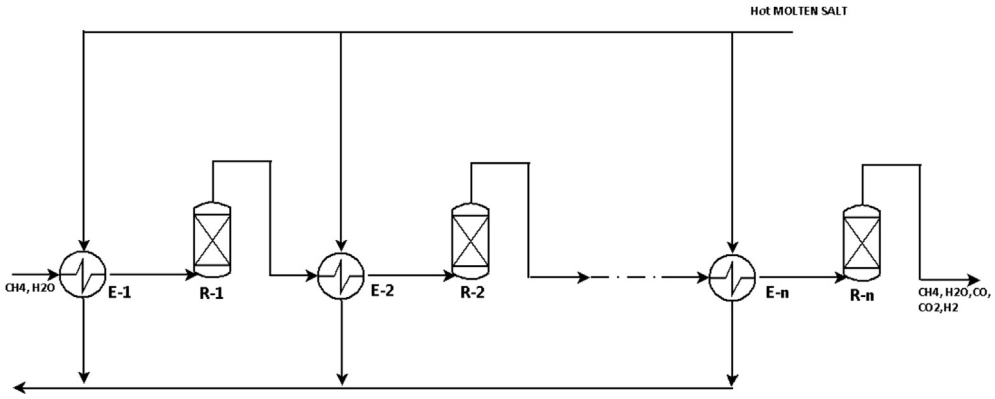

Fig. 4 – Heat Exchanger (E-i) + Reactor (R-i) series in the EHE configuration.

the CO content, to the condensation of the un-reacted water, to the PROX reactor to convert the trace of residual CO and the amine absorption unit to separate carbon dioxide. Also in this case, heat from water condensation and WGS reaction is recovered and used to produce the steam required for the reforming; furthermore, the outlet stream of molten salts is sent to the electricity generation unit to recover the residual sensible heat.

In both the configuration, the core of the process is the steam reforming reactor and, in order to properly simulate the process behavior, a rigorous model of the reactor has to be implemented. In the next paragraph, a two-dimensional (2D) reactor model is presented and described.

Reactor modeling

A reactor design tool is developed with a 2D mathematical model based on mass, energy and momentum balances [12,18] with the following assumptions:

- steady-state conditions;
- negligible axial and radial dispersion;
- pseudo-homogeneous behavior (gas and solid phases in the reactor are modeled as a single phase);
- ideal gas behaviour;
- a single tube representative of any other tube.

Steady state conditions can be assumed since the reactor is heated up by the molten salt stream pumped from the hot storage buffer (Fig. 2), which is designed with the scope to avoid the operative fluctuation of the chemical process.

In the following paragraphs, the model equations and the boundary conditions are reported; while the reaction kinetics are described in paragraph 3.3.

It is worth noting that no radial gradient appears in the adiabatic reactors of EHE configuration; therefore in this case a simpler 1D version of the model could be used.

Model equations

Model equations are obtained by imposing the mass, energy and momentum balances.

Mass Balances:

$$\frac{\partial(\tilde{u}_z\tilde{c}_i)}{\partial\tilde{z}} = \frac{d_p\cdot L}{Pe_{mr}\cdot R_i^2}\cdot\left(\frac{\partial^2(\tilde{u}_z\tilde{c}_i)}{\partial\tilde{r}^2}+\frac{1}{\tilde{r}}\cdot\frac{\partial(\tilde{u}_z\tilde{c}_i)}{\partial\tilde{r}}\right)-\frac{\rho_{cat}\cdot(1-\varepsilon)\cdot L}{u_{z,in}c_{CH_4,in}}\cdot\sum_{j=1}^{2}\nu_{ji}r_j \tag{3}$$

where R_i and L are the internal radius and the length of the reformer, $\tilde{z}$ and $\tilde{r}$ are the axial and radial dimensionless co-ordinates ($\tilde{z}=z/L$, $\tilde{r}=r/R_i$), $\tilde{u}_z$ and $u_{z,in}$ are the dimensionless gas velocity and its inlet value, $\tilde{c}_i$ and $c_{CH_4,in}$ the dimensionless i component concentration ($i=CH_4,H_2O,CO,CO_2,H_2$) and the inlet methane concentration, r_j is the observed reaction rate of the component i in the reaction j according to kinetic model described in paragraph 3.3, υ_{ij} is the stoichiometric coefficient of the component i for the reaction j, ρ_{cat} is the catalyst density, ε is the bed void fraction, d_p is the catalyst particle diameter.$Pe_{mr}=u_z d_p/D_{er}$ is the mass effective radial Pèclet number with the dispersion coefficient D_{er} calculated according to [19].

- Energy balance

$$\frac{\partial\tilde{T}_R}{\partial\tilde{z}} = \frac{\lambda_{er}\cdot L}{(u_z c_{tot})\cdot c_{p,mix}\cdot R_i^2}\cdot\left(\frac{\partial^2\tilde{T}_R}{\partial\tilde{r}^2}+\frac{1}{\tilde{r}}\cdot\frac{\partial\tilde{T}_R}{\partial\tilde{r}}\right) + \frac{\rho_{cat}\cdot(1-\varepsilon)\cdot L\cdot\sum_{j=1}^{2}\eta_j\cdot\left(-\Delta H_j\right)\cdot r_j}{(u_z c_{tot})\cdot c_{p,mix}\cdot T_{R,in}} \tag{4}$$

where $\tilde{T}_R$ and $T_{R,in}$ are the dimensionless and the inlet reactor temperature, $c_{p,mix}$ is the gas mixture specific heat, η_j, $(-\Delta H_j)$ and r_j are the effectiveness factor, the enthalpy and rate of the reaction j ($j=1,2$).

The effective radial thermal conductivity λ_{er}, i.e. the thermal conductivity of the pseudo-homogeneous phase (gas mixture + solid catalyst particles) is calculated according to [20] that, although concerning pseudo-homogeneous models, results widely suitable for the simulation of packed bed reactor heat transport.

Only for IHE configuration, also the energy balance for the molten salt stream into the shell has to be considered; assuming a co-current heating configuration:

$$\frac{d\tilde{T}_{MS}}{d\tilde{z}} = \frac{U\cdot L}{w_{MS}\cdot c_{p,MS}}\left(\tilde{T}_{MS}-\tilde{T}_R\right)\cdot 2\pi\cdot R_i \tag{5}$$

where $\tilde{T}_{MS}$, w_{MS} and $c_{p,MS}$ are the dimensionless temperature, the mass flow-rate and the specific heat of the molten salt stream. The overall heat transport coefficient U is calculated as:

$$U = \left[\frac{1}{h_{MS}}\cdot\frac{R_i}{R_o} + \frac{t_{met}}{k_{met}} + \frac{1}{h_W}\right]^{-1} \quad (6)$$

where R_o is the external radius of the reformer tube, h_{MS} is the heat transport coefficient in the molten salt side given by Ref. [21], t_{met} and k_{met} are the metal tube thickness and conductivity, respectively; h_W is the wall-to-fluid heat transport coefficient, evaluated as the usual heat transport coefficient of an unmixed layer near the wall [22,23]. It is worth noting that no radial temperature gradients are considered in the molten salts.

For EHE configuration, where molten salts are used to preheat the feed to each reactor, the molten salts outlet temperatures are evaluated according to the heat balance of the heat exchanger. In this work, it is assumed that the total molten salt flow-rate is equally divided among the heat exchangers E-i (see Fig. 4).

- Momentum balance

$$\frac{d\tilde{P}}{d\tilde{z}} = \frac{f\cdot G\cdot\mu_g\cdot L}{\rho_g\cdot d_p^2\cdot P_{in}}\cdot\frac{(1-\varepsilon)^2}{\varepsilon^3} \quad (7)$$

where $\tilde{P}$ and P_0 are the dimensionless and the inlet reaction pressure. The friction factor f is calculated by the well-known Ergun equation.

The IHE reactor 2D model is composed by the PDEs set (3), (4), (5) and (7) while the EHE reactor model is composed by the equations (3), (4) and (7).

Boundary conditions

Boundary conditions to solve the stationary PDEs set (one in the inlet section $\tilde{z} = 0$ and two for the radial coordinate $\tilde{r} = 1$ and $\tilde{r} = 0$) are reported as follow:

- Inlet section conditions ($\tilde{z} = 0, \forall\tilde{r}$)

$$\tilde{u}_z\tilde{c}_{CH_4} = 1 \quad (8)$$

$$\tilde{u}_z\tilde{c}_i = \frac{u_z c_i}{u_{z,0}c_{CH_4,in}} \quad (i = H_2O, H_2, CO, CO_2) \quad (9)$$

$$\tilde{T}_R = 1 \quad (10)$$

$$\tilde{P} = 1 \quad (11)$$

$$\tilde{T}_{MS} = \frac{T_{MS,inlet}}{T_{R,in}} \quad \left(\text{only for IHE configuration}\right) \quad (12)$$

where $T_{MS,inlet}$ is the molten salt temperature in the reactor R-1 inlet (refer to Fig. 3), after the pre-heating exchanger (E-1).

- Conditions on reformer tube wall ($\tilde{r} = 1, \forall\tilde{z}$)

$$\frac{\partial(\tilde{u}_z\tilde{c}_i)}{\partial\tilde{r}} = 0 \quad (13)$$

Concerning the energy boundary condition, for IHE it has to be imposed that a heat flux is supplied by the hot molten salt stream from the shell:

$$\lambda_{er}\frac{\partial\tilde{T}_R}{\partial\tilde{r}} = \frac{q_r\cdot R_i}{T_{R,0}} = U\cdot R_i\left(\tilde{T}_{MS} - \tilde{T}_R\big|_{Ri}\right) \quad (14)$$

where q_r is the heat flux from the molten salt to the reactor packed bed.

On the other hand, in the EHE configuration the reactor is adiabatic and the boundary condition on reformers tube wall is:

$$\frac{\partial\tilde{T}_R}{\partial\tilde{r}} = 0 \quad (15)$$

- Conditions on reformer tube axis ($\tilde{r} = 0, \forall\tilde{z}$)

$$\frac{\partial(\tilde{u}_z\tilde{c}_i)}{\partial\tilde{r}} = 0 \quad (16)$$

$$\frac{\partial\tilde{T}_R}{\partial\tilde{r}} = 0 \quad (17)$$

In conclusion, the boundary conditions for IHE reactor are (8–14), (16) and (17), while for EHE reactor are (8–11), (13) and (15–17).

Reactions kinetics

The simulation of methane steam reforming process requires an accurate description of the chemical kinetics of the reactions on the specific catalyst used.

The chemical kinetics of methane steam reforming are widely described in literature. The Xu-Froment model [24] has been widely used to describe the steam reforming kinetics; however this model requires the knowledge of both kinetic parameters and adsorption equilibrium constants; furthermore this model is inconsistent at zero hydrogen pressure. In recent years Wei and Iglesia suggested a simpler kinetics model [25], including just one kinetics parameter.

Kinetics model

The Wei-Iglesia study [25] considers that the rate determining step is the activation of the strong C–H bond of the methane molecule both for steam reforming or dry reforming process. The other reforming steps and the water gas shift are considered as equilibrium reactions. This assumption is supported by several WGS experimental data reported in the literature. Furthermore it is worth noting that, at the operating temperatures considered in the simulations, the WGS conversion is very high and the CO concentration is extremely low, as shown in Fig. 7.

Therefore, the direct steam reforming reaction kinetics is assumed to be proportional to the methane partial pressure; experimental data show that water, carbon dioxide or

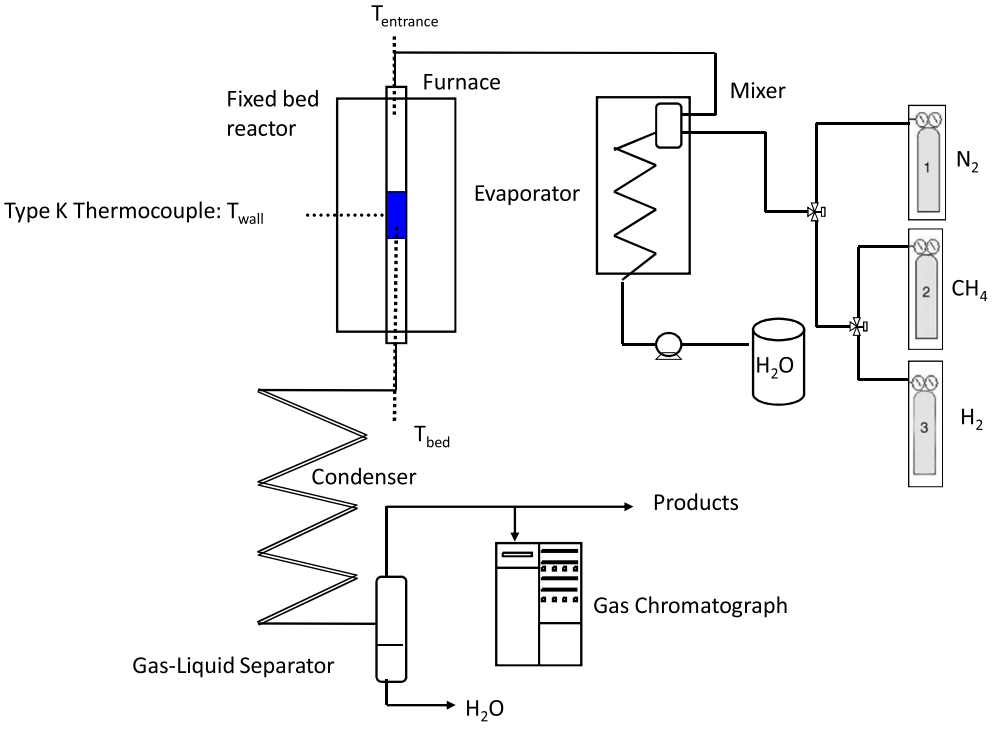

Fig. 5 – Experimental test bench layout.

hydrogen concentrations do not affect the methane conversion kinetics. According to this model, kinetics of steam reforming is written as:

$$r_{SR} = k \cdot p_{CH_4} \cdot (1 - \eta) \tag{18}$$

where $(1-\eta)$ is a parameter that indicates the distance from equilibrium given by (19)

$$\eta = \frac{1}{K_{SR}} \frac{p_{CO} \cdot p_{H_2}^3}{p_{CH_4} \cdot p_{H_2O}} \tag{19}$$

K_{SR} is the equilibrium constant of steam reforming and p_{CO}, p_{H2}, p_{CH4} and p_{H2O} are the partial pressures of CO, H_2, CH_4 and H_2O respectively. In the present work, the parameter k, introduced in equation (23), is considered as an apparent kinetic constant that can be obtained from the fitting of the experimental data.

It is worth noting that hydrogen and water partial pressures do not influence the direct reaction kinetics, but they appear in η term and then affect the overall reaction rate. Furthermore, CO, CO_2, water and hydrogen composition is evaluated accounting for the simultaneous gas shift reaction; as previously reported, this reaction is assumed to reach the equilibrium conditions so that the relation

$$K_{WGS} = \frac{p_{CO_2} \cdot p_{H_2}}{p_{CO} \cdot p_{H_2O}} \tag{20}$$

must be satisfied. In this case, it can be proved that the WGS rate can be expressed as:

$$r_{WGS} = r_{SR} \frac{K_{WGS}(P_{H_2O} - P_{CO}) - 3P_{CO_2}}{K_{WGS}(P_{H_2O} + P_{CO}) + P_{H_2} + P_{CO_2}} \tag{21}$$

According to this approach, just one parameter k is required in order to describe the process kinetics.

Experimental reactor and parameter estimation

In this work, some experiments have been carried out to test a Nickel (54% wt) based commercial catalyst (BASF G1-85 5 × 5 mm), supported by Al_2O_3 (20% wt) for low temperature steam reforming and evaluate the kinetic constant defined in eq. (24).

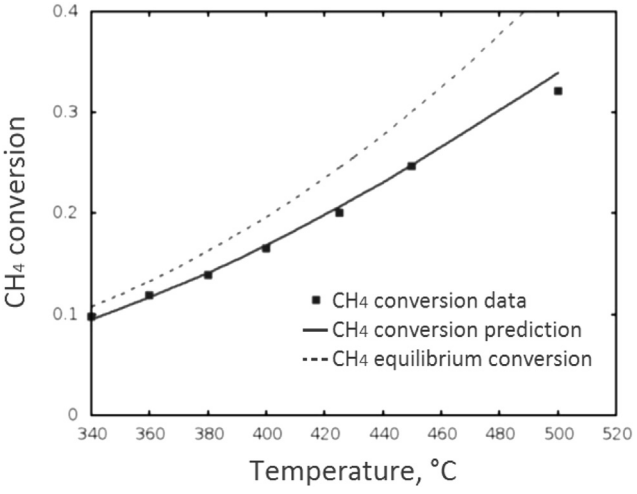

Fig. 6 – Comparison between experimental, calculated and equilibrium methane conversion within the operating temperature range 340–500 °C.

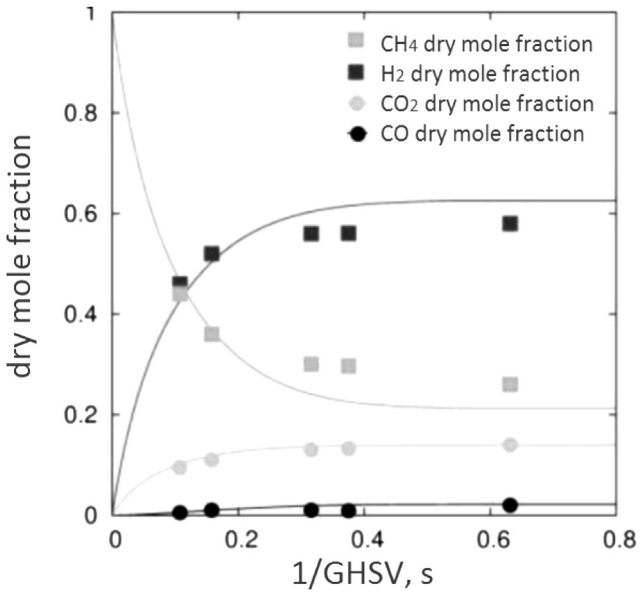

Fig. 7 – Experimental and calculated mixture composition vs. GHSV.

Tests of the reforming catalyst for low temperature steam reforming is carried out in a laboratory fixed-bed reactor under atmospheric pressure at different temperature and GHSV. Fig. 5 shows a test-bench layout. The catalyst is placed in a quartz reactor with an inner diameter of 15.5 mm heated up in an electric furnace; A K-type thermocouple is directly inserted into the catalyst bed to measure the reactor temperature. The reactor can be fed with gas at different compositions and steam produced in the evaporator. At the exit the reactor, the water is condensed and separated from the gas phase which is analyzed with an online portable chromatograph Varian CP-4900, equipped with a molecular sieve column and TCD detector.

The nickel catalyst is supplied as supported nickel oxide and it must be reduced to give the active metallic nickel. The reduction is carried out with a mixture of nitrogen and hydrogen (25% vol. H_2) for 6–8 h. After the reduction, the reformer is brought on-line switching the feed from the hydrogen–nitrogen mixture to the natural gas. The initial natural gas rate is set to 25% of the set point value and the steam-to-carbon ratio (S/C) is set to 5; then, the natural gas flow rate is increased until the desired S/C ratio is reached.

Typical example of experimental data in terms of methane conversion and outlet mixture composition are reported in Figs. 6 and 7.

Experimental data are compared with the methane conversion calculated according to the Wei and Iglesia model:

$$\frac{1}{k}\int_0^{X_{CH_4}} \frac{dX'_{CH_4}}{p_{CH_4}\cdot(1-\eta)} = \frac{V}{F^0_{CH_4}} = \frac{1+S/C}{GHSV}\frac{RT_s}{P_s} \tag{22}$$

where R is the gas constant, GHSV is the gas hourly space velocity at standard temperature (T_s) and pressure (P_s). In the above equation the mixture composition that appear in η is obtained assuming the equilibrium of water gas shift reaction.

The kinetic constant k is then evaluated comparing the model simulations with the experimental data of methane conversion obtained at 101 kPa, GHSV = 9300 h^{-1}, S/C = 3 and temperature ranging from 340 °C to 500 °C. The values of k so determined are correlated by Arrhenius equation, obtaining a value of kinetic constant at 500 °C equal to 12,140 mol/m^3 s atm and an activation energy E_a/R = 4200 K:

$$k = 12140\cdot\exp\left(-\frac{4200}{T}\right) \tag{23}$$

Fig. 6 shows the comparison between experimental and calculated methane conversion data: the agreement is good for each temperature.

To test the model, experiments at 500 °C and different GHSV in the range of 5700 h^{-1} and 33,500 h^{-1} have been carried out and the dry composition of the gas from the reactor is compared with the model prediction. The comparison seems to be quite satisfactory in the whole GHSV range (see Fig. 7).

Therefore, Wei-Iglesia model, with the parameters previously determined, is used in the low temperature reformer mathematical model to compare the performance of EHE and IHE reactors.

Table 1 – Solar steam reforming plant operating parameters.

Inlet methane flowrate Q_{CH_4}	100–500 Nm^3/h
H_2 %vol in the outlet stream	20%
Hot molten salt temperature (after CSP plant)	823 K
Operating reaction pressure	15 bar
Reforming catalyst density	1990.6 kg/m^3
Reactor void fraction ε	$\varepsilon = 0.6885\cdot\frac{d_{part}}{2\cdot R_i} + 0.30675$ [26]
Catalyst particle diameter d_p	$d_o = 0.016$m $d_i = 0.006$m $h_c = 0.016$m $d_p = 6\cdot\left\{\left[\frac{0.25\cdot h_c\cdot(d_o-d_i)}{h_c+0.5\cdot(d_o-d_i)}\right]\right\}$m
Molten salt stream velocity v_{MS}	0.8545 m/s
Molten salt flowrate w_{MS}	8.96 kg/s
Molten salt density ρ_{MS}	$\rho_{MS} = 2090 - 0.636\cdot(T_{MS} - 273.15)$ kg/m^3

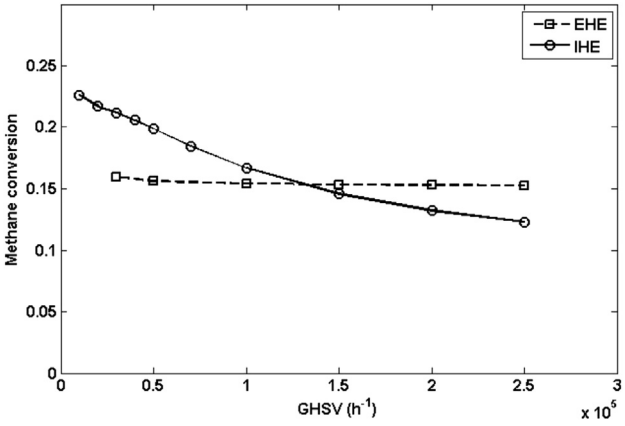

Fig. 8 – Methane conversion vs. GHSV for EHE and IHE configurations (Q_{CH4} = 100 Nm^3/h; S/C = 3; T_{in} = 793 K).

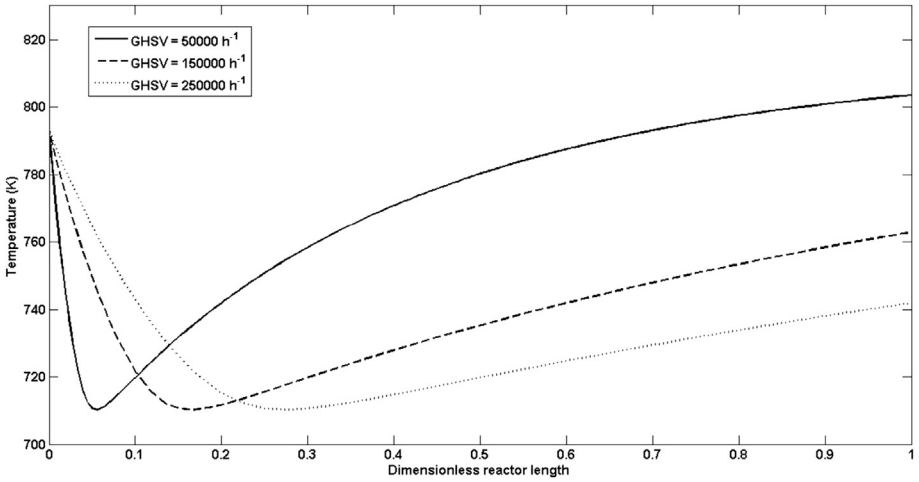

Fig. 9 – Mean temperature profile inside IHE reactor for GHSV = 50000 h^{-1}, 150000 h^{-1}, 250000 h^{-1} (Q_{CH4} = 100 Nm^3/h; S/C = 3; T_{in} = 793 K).

Results and discussion

The IHE and EHE configurations are simulated fixing the operating parameters listed in Table 1 and varying the inlet GHSV, the inlet reactant temperature and the steam to carbon ratio (S/C) in the reactor feedstock. Then, the influence of increasing the chemical plant size, i.e. increasing the inlet methane flow-rate fixing the solar plant size, is assessed.

Concerning with the EHE configuration, the maximum number of assembled reactors has been fixed at three, in order to avoid an excessive plant complexity.

Effect of GHSV

Firstly, the effect of GHSV on solar reformer performance is analyzed. The GHSV is varied keeping constant the inlet feedstock (100 Nm^3/h of CH_4, S/C = 3) and the reactor inner diameter (8 reformers with internal diameter = 3.56 cm) and varying the reformers length.

Fig. 8 shows the reformers methane conversion X_{CH4} varying the GHSV for EHE and IHE: it is a worth assessment that while the reactant conversion is almost constant for EHE, since equilibrium conditions are achieved at the outlet of each adiabatic reformer, the conversion in the integrated reactor strongly depends on GHSV. In fact, even if also in this case the equilibrium conversion is achieved at the outlet of the reformer, the reduction of the GHSV leads to an increase of mixture outlet temperature and, consequently, of the endothermic steam reforming reaction conversion; this result suggests that the limiting step for the methane conversion is the heat exchange from the molten salt stream to the packed bed instead of the reactions kinetics. Fig. 9 shows the mean temperature profiles for IHE reactor at GHSV of 50,000 h^{-1}, 150,000 h^{-1} and 250,000 h^{-1}, while Fig. 10 illustrates the typical profile in the EHE adiabatic reactor: in the IHE reactor, the final methane conversion strictly depends on the final gas mixture temperature $T_{R,out}$ (X_{CH4} = 0.2 and $T_{R,out}$ = 802 K at 50,000 h^{-1}, X_{CH4} = 0.146 and $T_{R,out}$ = 761 K at 150,000 h^{-1}, X_{CH4} = 0.123 and $T_{R,out}$ = 741 K at 250,000 h^{-1}); on the other hand, in the EHE the gas mixture reaches the equilibrium condition and

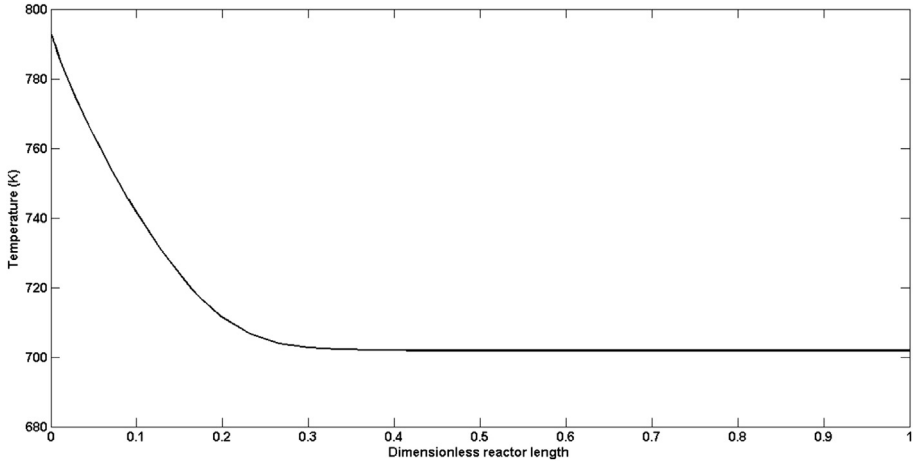

Fig. 10 – Mean temperature profile inside EHE reactor for GHSV = 250000 h^{-1} (Q_{CH4} = 100 Nm^3/h; S/C = 3; T_{in} = 793 K).

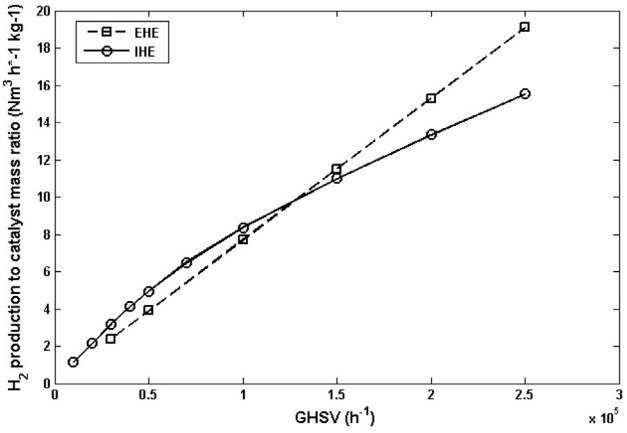

Fig. 11 – H_2 production to catalyst mass ratio vs. GHSV (Q_{CH4} = 100 Nm^3/h; S/C = 3; T_{in} = 793 K).

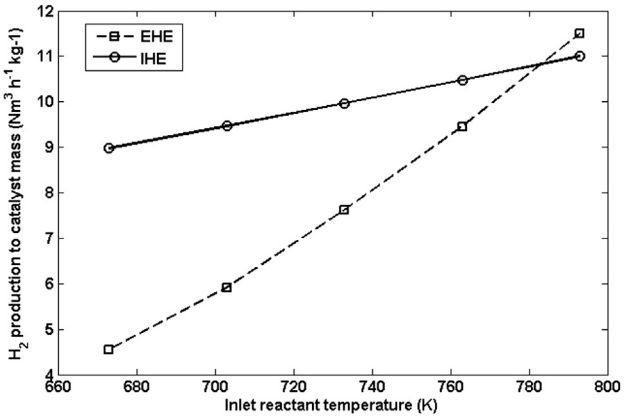

Fig. 13 – H_2 production to catalyst mass ratio vs. inlet reactants temperature (Q_{CH4} = 100 Nm^3/h; S/C = 3; GHSV = 150000 h^{-1}).

consequently the temperature tends to a constant value depending on the reactor inlet temperature and inlet reactants mixture composition.

Globally, at simulated operating conditions, the IHE allows a greater conversion than EHE when the GHSV is lower than 130,000 h^{-1} approximately, while the EHE leads to a higher reactant conversion when the GHSV is higher.

Fig. 11 reports the catalyst productivity (defined as the ratio between the H_2 production rate and the catalyst mass) as a function of the GHSV for IHE and EHE: while for the EHE reactor the catalyst productivity increases linearly, the productivity in the IHE shows a non linear behavior. However, for both the configurations the catalyst productivity increases at higher GHSV, although the methane conversion is lower: at the highest GHSV considered (250,000 h^{-1}) the productivity is 19.1 Nm^3 h^{-1} kg^{-1} for EHE and 15.5 Nm^3 h^{-1} kg^{-1} for IHE.

The flow rate of the enriched methane (20% vol. H_2) obtained from the reformer ranges from 398 Nm^3/h to 249 Nm^3/h at 50,000 h^{-1} and 250,000 h^{-1} respectively for IHE configuration, and it is almost constant (about 308 Nm^3/h) for EHE configuration.

Effect of inlet reactant temperature

Fig. 12 shows the dependence of methane conversion on the inlet reactor temperature $T_{R,in}$. Being the steam reforming process strongly endothermic, the conversion increases when the temperature is higher.

The EHE reactor performance is more affected by the inlet temperature (methane conversion equal to 0.06 at $T_{R,in}$ = 673 K and to 0.154 at $T_{R,in}$ = 793 K, with an increase of +157%) than the IHE one (methane conversion equal to 0.118 at $T_{R,in}$ = 673 K and to 0.146 at $T_{R,in}$ = 793 K, +23.7%). Concerning with the catalyst productivity (Fig. 13), the trends are similar to those of methane conversion: for the EHE configuration, the productivity is 4.55 Nm^3 h^{-1} kg^{-1} at 673 K and 11.5 Nm^3 h^{-1} kg^{-1} at 793 K, while for the IHE reactor is 8.98 Nm^3 h^{-1} kg^{-1} at 673 K and 11 Nm^3 h^{-1} kg^{-1} at 793 K (+22.5%). The reason is that the inlet feedstock enthalpy, which depends on $T_{R,in}$, is the only energy amount supplied to the reactor for the EHE configuration, thus strongly affecting the reactions performance, while in the IHE reformer the reactions are continuously supported by the heat flow from the molten salt stream to the

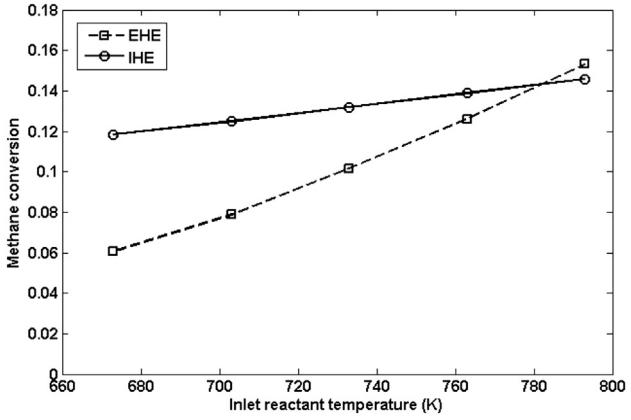

Fig. 12 – Methane conversion at various inlet reactant temperature (Q_{CH4} = 100 Nm^3/h; S/C = 3; GHSV = 150000 h^{-1}).

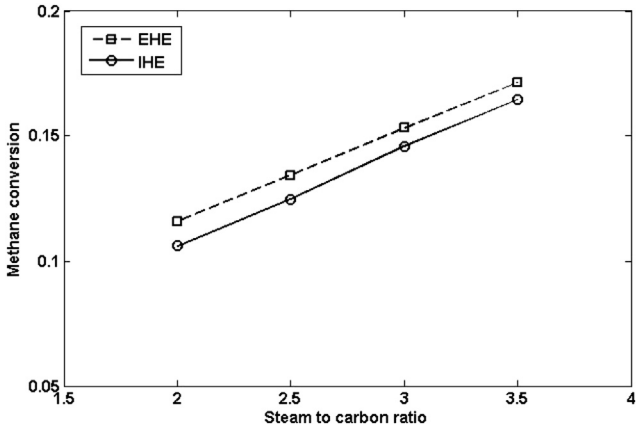

Fig. 14 – Methane conversion varying the steam to carbon ratio in the inlet feedstock (Q_{CH4} = 100 Nm^3/h; GHSV = 150000 h^{-1}; T = 793 K).

Table 2 – Methane conversion and molten salt temperature after pre-heating (heat exchanger E-1 at Fig. 3 and E-1 at Fig. 4) at various inlet methane flow-rate (GHSV = 150000 h^{-1}, S/C = 3, T_{in} = 793 K).

Methane flow-rate (Nm^3/h)	T_{MS} after pre-heating in IHE configuration (K)	IHE methane conversion	T_{MS} after pre-heating in EHE configuration (K)	EHE reactors methane conversion
100	818.07	0.146	816.31	0.153
400	802.84	0.135	795.78	0.153
700	787.6	0.126	775.25	0.153
1000	772.39	0.117	754.72	0.153
2000	721.6	0.093	686.29	0.153

catalyst packed bed and, consequently, the inlet enthalpy is only a small share of the total supplied energy .

Effect of steam to carbon ratio

The steam to carbon ratio effects on methane conversion are reported in Fig. 14 at constant methane flow rate and GHSV value. Obviously the higher S/C ratio, the higher the methane conversion for both reactor configuration. On the other hand it is worth noting that the increase of S/C ratio requires an increase of the reactor volume, in order to keep a constant GHSV value.

Therefore while the S/C ratio strongly affects the methane conversion, it has only a minor effect on the reactor productivity. In particular an increase of the S/C ratio from 2 to 3.5 results in an increase of methane conversion equal to 46% for EHE and 55% for IHE while the productivity increases of only of about 1% for EHE and 3% for IHE.

Effect of inlet methane flow-rate

Finally, the effect of increasing the inlet methane to be treated by the steam reforming plant, fixing the solar plant size, i.e. the hot molten salt stream flow rate and temperature, is evaluated (see Table 2). In particular both the enriched methane production and the electric power produced by exploiting the residual enthalpy of the molten salt stream (with a conversion efficiency equal to 28%) has been considered. The simulation results are reported in Figs. 15 and 16, for inlet methane flow-rate varying in the range 100–2000 Nm^3/h.

Clearly the higher the methane flow rate, the higher the EM production and the lower the electrical power production. In details it should be pointed out that while the EM production increases almost linearly for EHE configuration, in the IHE configuration the increase is lower at higher methane flow rate. This result is due to the process configuration utilized with the IHE reactor. In fact, in this case, the higher the methane flow rate, the higher the thermal duty in the heat exchanger E–1 and the lower the temperature of the outlet molten salt used to heat the IHE reactor. As reported in Table 2, the reduction of the molten salt temperature results in a reduction of the methane conversion in the IHE. On the other hand the configuration used with EHE reactors allows to heat up to 793 K the gas streams fed to each reactor and the methane conversion is practically unaffected by the methane flow rate.

As previously reported, as for the electrical power, the trends are opposite: greater the enriched methane production, lower the electrical power since lower the availability of the molten salt enthalpy, as reported in Table 2. Globally, when 2000 Nm^3/h of natural gas are treated by the plant, 6132.9 Nm^3/h of enriched methane and 476 kW_{el} are produced implementing the EHE configuration, 3721 Nm^3/h and 585.6 kW_{el} are produced with IHE configuration.

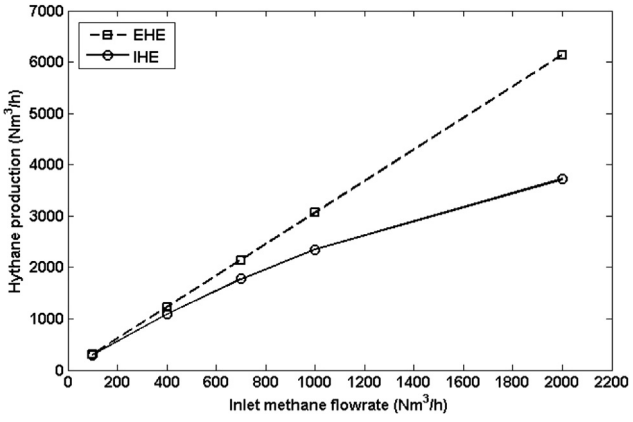

Fig. 15 – Hydrogen/methane mixture production (20% vol. H_2) at various inlet methane flowrate (GHSV = 150000 h^{-1}, S/C = 3, T_{in} = 793 K).

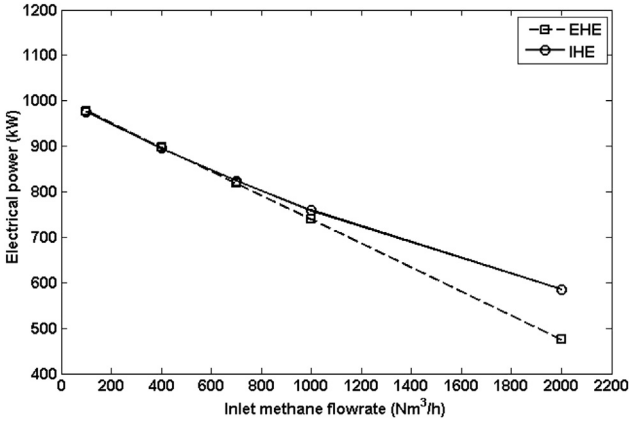

Fig. 16 – Electrical power production (conversion efficiency of the turbine equal to 28%) at various inlet methane flowrate (GHSV = 150000 h^{-1}, S/C = 3, T_{in} = 793 K).

Conclusions

An EM production plant, based on a low-temperature steam reforming process heated up a MS-CSP, has been studied.

Two steam reforming reactor configurations have been modeled : the Integrated Heat Exchanging (IHE) configuration, where the steam reformers are tubes-and-shell reactors continuously heated up by the hot MS stream, and the External Heat Exchanging (EHE) configuration composed by a series of heat exchangers and insulated reformers where the reactions are adiabatically driven. Simulations have been carried out to study the influence of some operating conditions like GHSV, inlet temperature and inlet reactant composition.

The results show that, globally, the EM production is supported by increasing the GHSV, even if the methane conversion is reduced, and by increasing the inlet reaction temperature, whose effect is more evident for the EHE than for the IHE reactor. On the contrary the inlet steam to carbon ratio doesn't significantly affect the productivity.

Including an electrical power generation unit, able to exploit the enthalpy of the residual MS stream after the EM production unit to generate electricity, the plants produce, with a feed of 2000 Nm^3/h of natural gas, 6130 Nm^3/h of enriched methane (H_2 20%vol.) and 475 kW_{el} with the EHE configuration, 3720 Nm^3/h and 585 kW_{el} with IHE configuration.

The work has demonstrated the feasibility of the technology and the good match between a solar plant and an endothermic chemical process able to exploit the solar energy to produce hydrogen.

Acknowledgment

This work has been carried out within the framework of the project METISOL "Produzione di miscele METano-Idrogeno con cicli termochimici alimentati da energia SOLare e sistemi di stoccaggio a bordo veicolo", financially supported by Italian Environment Ministry (G.U 299, 23/12/2008).

Nomenclature

$c_{CH_4,in}$	inlet methane concentration, kmol m^{-3}
$\tilde{c}_i$	dimensionless *i* component concentration
$c_{p,mix}$	gas mixture specific heat, kJ $kmol^{-1}$ K^{-1}
$c_{p,MS}$	molten salt specific heat, kJ $kmol^{-1}$ K^{-1}
d_p	catalyst particle diameter, m
EHE	External Heat Exchanging
EM	Enriched Methane
f	friction factor
GHSV	Gas Hourly Space Velocity, h^{-1}
h_{MS}	heat transport coefficient in the molten salt side, kJ h^{-1} K^{-1} m^{-2}
h_W	tube wall-to-fluid heat transport coefficient, kJ h^{-1} K^{-1} m^{-2}
$(-\Delta H_j)$	enthalpy of the reaction *j*, kJ mol^{-1}
IHE	Integrated Heat Exchanging
k	kinetics constant
K_j	equilibrium constant of reaction *j*
k_{met}	metal tube conductivity, kJ h^{-1} K^{-1} m^{-1}
L	reactor length, m
MS	molten salt
MS-CSP	Molten Salt Concentrating Solar Plant
NG-ICE	Natural Gas Internal Combustion Engines
$\tilde{P}$	dimensionless reaction pressure.
p_i	*i* component partial pressure, bar
P_0	inlet reaction pressure, bar
Pe_{mr}	Mass effective radial Pèclet number
Q_{CH_4}	inlet methane flow-rate, Nm^3 h^{-1}
q_r	heat flux from the molten salt to the reactor packed bed, kJ h^{-1} m^{-2}
$\tilde{r}$	dimensionless radial coordinate
r_j	observed rate of the reaction *j*, kmol h^{-1} kg^{-1}
R_i	reactor internal radius, m
R_o	external radius of the reformer tube, m
t_{met}	metal tube thickness, m
$\tilde{T}_{MS}$	dimensionless molten salt temperature
$T_{MS,inlet}$	molten salt temperature in the reactor shell, K
$\tilde{T}_R$	dimensionless reactor temperature
$T_{R,in}$	inlet reaction temperature, K
$T_{R,out}$	outlet reaction temperature, K
S/C	steam to carbon ratio
SR	Steam Reforming
U	overall heat transport coefficient, kJ h^{-1} K^{-1} m^{-2}
$\tilde{u}_z$	dimensionless gas velocity
$u_{z,in}$	inlet gas velocity, m s^{-1}
v_{MS}	molten salt mass velocity, m s^{-1}
X_{CH4}	methane conversion
w_{MS}	molten salt mass flow-rate, kg h^{-1}
WGS	Water Gas Shift
$\tilde{z}$	dimensionless axial coordinate

Greek symbols

ε	reactor bed void fraction
η_j	catalyst effectiveness factor
λ_{er}	effective radial thermal conductivity, kJ h^{-1} K^{-1} m^{-1}
ρ_{cat}	catalyst density, kg m^{-3}
ρ_{MS}	molten salt density, kg m^{-3}

REFERENCES

[1] Ortenzi F, Chiesa M, Scarcelli R, Pede G. Experimental tests of blends of hydrogen and natural gas in light-duty vehicles. Energy 2008;33:3225–9.

[2] Bauer CG, Forest TW. Effect of hydrogen addition on the performance of methane-fueled vehicles. Part I: effect of S.I. engine performance. Int J Hydrogen Energy 2001;26:55–70.

[3] Bauer CG, Forest TW. Effect of hydrogen addition on the performance of methane-fueled vehicles. Part II: driven cycle simulations. Int J Hydrogen Energy 2001;26:71–90.

[4] Yon S, Sautet JC. Flame lift-off height, velocity flow and mixing of hythane in oxy-combustion in a burner with two separated jets. Appl Therm Eng 2012;32:83–92.

[5] Larsen JF, Wallace JS. Comparison of emissions and efficiency of a turbocharged lean-burn natural gas and hythane-fueled engine. J Eng Gas Turbines Power 1997;119:218–26.

[6] Orhan Akansu S, Dulger Z, Kaharaman N, Veziroglu TN. Internal combustion engines fuelled by natural gas–hydrogen mixtures. Int J Hydrogen Energy 2004;29:1527–39.
[7] Haeseldonckx D, D'haeseleer W. The use of natural-gas pipeline infrastructure for hydrogen transport in a changing market structure. Int J Hydrogen Energy 2007;32:1381–6.
[8] De Falco M, Basile A. Special section – hydrogen enriched methane: editorial. Int J Hydrogen Energy 2012;37:10973.
[9] Cavinato C, Giuliano A, Bolzonella D, Pavan P, Cecchi F. Biohythane production from food waste by dark fermentation coupled with anaerobic digestion process: a long-term pilot scale experience. Int J Hydrogen Energy 2012;37:11549–55.
[10] Pawar SS, Nkongndem Nkemka V, Zeidan AA, Murto M, van Niel EWJ. Biohydrogen production from wheat straw hydrolysate using caldicellulosiruptor saccharolyticus followed by biogas production in a two-step uncoupled process. Int J Hydrogen Energy 2013;38:9121–30.
[11] Liu Z, Zhang C, Lu Y, Wu X, Wang L, Wang L, et al. States and challenges for high-value biohythane production from waste biomass by dark fermentation technology. Bioresour Technol 2013;135:292–303.
[12] De Falco M, Giaconia A, Marrelli L, Tarquini P, Grena R, Caputo G. Enriched methane production using solar energy: an assessment of plant performance. Int J Hydrogen Energy 2009;34:98–109.
[13] Piemonte V, De Falco M, Giaconia A, Basile A, Iaquaniello G. Production of enriched methane by a molten salt concentrated solar power plant coupled with a steam reforming process: an LCA study. Int J Hydrogen Energy 2012;37:11556–61.
[14] Rostrup-Nielsen JR. Production of synthesis gas. Catal Today 1993;18:305–24.
[15] Pacheco JE, Showalter SK, Kolb WJ. Development of a molten-salt thermocline thermal storage system for parabolic trough plants. ASME J Sol Energy Eng 2002;124:153–9.
[16] Mills D. Advances in solar thermal electricity technology. Sol Energy 2004;76:19–31.
[17] Herrmann U, Kelly B, Price H. Two-tank molten salt storage for parabolic trough solar power plants. Energy 2004;29:883–93.
[18] De Falco M. Innovative solar technology: CSP plants for combined production of hydrogen and electricity. In: Piemonte V, De Falco M, Basile A, editors. Sustainable development in chemical engineering. Wiley; 2013, ISBN 978-1-119-95352-4. pp. 25–49.
[19] Kulkarni BD, Doraiswamy LK. Estimation of effective transport properties in packed bed reactors. Catal Rev Sci Eng 1980;22(3):431–83.
[20] De Wasch AP, Froment GF. Heat transfer in packed beds. Chem Eng Sci 1972;27:567–76.
[21] Miliozzi A, Giannuzzi GM, Tarquini P, La Barbera A. Fluido termovettore: dati di base della miscela di nitrati di sodio e potassio, ENEA Report; ENEA/SOL/RD/2001/07.
[22] Tsotsas E, Schlunder E. Heat transfer in packed beds with fluid flow: remarks on the meaning and the calculation of a heat transfer coefficient at the wall. Chem Eng Sci 1990;45:819–37.
[23] Li C, Finlayson B. Heat transfer in packed beds – a reevaluation. Chem Eng Sci 1977;32:1055–66.
[24] Xu J, Froment GF. Methane steam reforming, methanation and water-gas shift: 1. Intrinsic kinetics. AIChE J 1989;35:88–96.
[25] Wei J, Iglesia E. Isotopic and kinetic assessment of the mechanism of reactions of CH_4 with CO_2 or H_2O to form synthesis gas and carbon on nickel catalysts. J Catal 2004;224:370–83.
[26] Leva M, Weintraub M, Grummer M, Pollchik M, Storch HH. Fluid flow through packed and fluidized systems. Bulletin 504, Bureau Mines; 1951.